Single-Molecule Magnets

Deutsche Ausgabe: DOI: 10.1002/ange.201604346
Internationale Ausgabe: DOI: 10.1002/anie.201604346

A Low-Symmetry Dysprosium Metallocene Single-Molecule Magnet with a High Anisotropy Barrier

*Thomas Pugh, Nicholas F. Chilton, and Richard A. Layfield**

Abstract: *The single-molecule magnet (SMM) properties of the isocarbonyl-ligated dysprosium metallocene $[Cp^*_2Dy\{\mu\text{-}(OC)_2FeCp\}]_2$ ($\mathbf{1_{Dy}}$), which contains a rhombus-shaped Dy_2Fe_2 core, are described. Combining a strong axial $[Cp^*]^-$ ligand field with a weak equatorial field consisting of the isocarbonyl ligands leads to an anisotropy barrier of 662 cm^{-1} in zero applied field. The dominant thermal relaxation pathways in $\mathbf{1_{Dy}}$ involves at least the fourth-excited Kramers doublet, thus demonstrating that prominent SMM behavior can be observed for dysprosium in low-symmetry environments.*

Over the last quarter of a century, single-molecule magnets (SMMs) have captivated the attention of chemists, physicists, and materials scientists.[1] SMMs are characterized by an effective energy barrier (U_{eff}) to reversal of their magnetization, and, in some cases, they also display magnetic hysteresis with remanence and coercivity.[2] The quantum magnetic properties and bistability of SMMs has led to these materials being proposed for applications in information storage,[3] and several examples have been employed as components in prototype molecular spintronic devices.[4]

A key driving force behind the development of SMMs is the synergic relationship between experiment and theory, which has produced a range of effective magneto-structural correlations, predominantly focused on 4f and 3d metals.[5] Significant enhancements in U_{eff} and in the blocking temperature (T_B) have arisen through careful use of such correlations,[6] which ultimately provides the inspiration for targeting new systems that could function at practical temperatures.

For lanthanide SMMs, dramatic improvements in U_{eff} can be achieved by engineering the multiplet structure of the spin-orbit coupled ground state using rationally designed coordination chemistry. In the case of dysprosium—the most popular lanthanide in SMMs—the strategy typically aims to install a strong axial crystal field and a weak equatorial field. Combining these properties in an SMM with a high-order principal symmetry axis can significantly stabilize the Kramers doublets (KDs) with the largest m_J values, leading to substantial increases in U_{eff}.[7]

[*] Dr. T. Pugh, Dr. N. F. Chilton, Prof. Dr. R. A. Layfield
School of Chemistry
The University of Manchester
Oxford Road, Manchester, M13 9PL (U.K.)
E-mail: Richard.Layfield@manchester.ac.uk
Supporting information and the ORCID identification number(s) for the author(s) of this article can be found under http://dx.doi.org/10.1002/anie.201604346.

We have focused on SMMs containing the dysprosium metallocene unit $\{Cp'_2Dy\}$ (Cp′ = substituted cyclopentadienyl),[8] that is, $[Cp'_2Dy(\mu\text{-}X)]_n$ ($n = 2$, 3) where the μ-X ligand contains a soft donor, for example, phosphorus, arsenic, sulfur or selenium.[9–12] U_{eff} values of up to 331 cm^{-1} have been determined for these and related metallocene SMMs.[13] Ab initio calculations have allowed us to propose a new magnetostructural correlation for these SMMs, whereby the ground KD is characterized by the $m_J = \pm 15/2$ wave-function, and the easy axis of magnetization is oriented towards the $[Cp]^-$ ligands (Scheme 1). Thus, the X ligands reside in the equatorial plane, and removing them from $[Cp_2Dy(\mu\text{-}X)]_n$ would eliminate the equatorial field and produce a pseudo-2-coordinate species $[Cp_2Dy]^+$. Removing the X ligands could also, on steric grounds, allow the angle θ to approach 180°, which would further enhance the axiality and maximize U_{eff}.

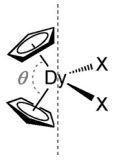

Scheme 1. Illustration of the easy axis of magnetization (dashed gray line) in the ground Kramers' doublet of a $\{Cp_2Dy\}$-containing SMM.

From a synthetic perspective, the large radius and highly electrophilic nature of Dy^{3+} render the formation of $[Cp_2Dy]^+$ (as a salt of a non-coordinating anion) a formidable challenge. An alternative strategy is to use X ligands that generate a very weak crystal field and that impose light steric demands. To achieve this, the isocarbonyl ligand—with its rod-like structure and low-lying oxygen-centered lone pair—is an excellent candidate. We now deploy the magnetostructural model in Scheme 1 to engineer a new isocarbonyl-ligated dysprosium SMM with one of the largest anisotropy barriers yet recorded.

The isocarbonyl ligands were installed into the dysprosium metallocene through the salt elimination reaction of $[Cp^*_2M(\mu\text{-}Ph)_2BPh_2]$ (M = Y, Dy; Cp* = pentamethylcyclopentadienyl) with K[Fp] (Fp = $CpFe(CO)_2$), resulting in the formation of $[Cp^*_2M(\mu\text{-}Fp)]_2$ (M = Y, $\mathbf{1_Y}$; M = Dy, $\mathbf{1_{Dy}}$) according to Scheme 2.

Complexes $\mathbf{1_Y}$ and $\mathbf{1_{Dy}}$ were isolated in yields of 73% and 77%, respectively, and their structures were determined by X-ray crystallography (Figures 1 and Figure S4, Tables S1,S2 in the Supporting Information).[14] The isostructural compounds crystallize as centrosymmetric dimers in the $P\bar{1}$ space group. Individual molecules of $\mathbf{1_Y}$ and $\mathbf{1_{Dy}}$ are D_{2h} symmetric, however the metal atoms occupy coordination environments that are close to C_{2v} symmetric, with two η^5-Cp* ligands and

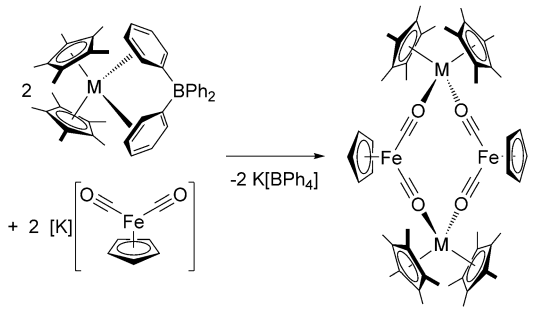

Scheme 2. Synthesis of compounds $\mathbf{1}_{M}$ (M = Y, Dy).

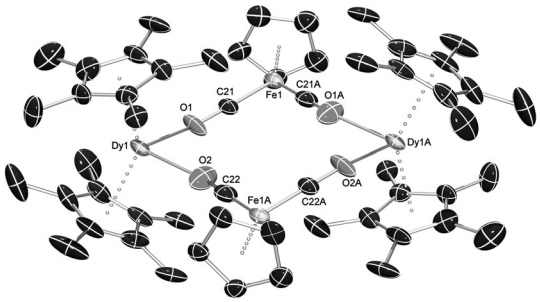

Figure 1. Molecular structure of $\mathbf{1}_{Dy}$ with thermal ellipsoids set at 50% probability. Hydrogen atoms not shown.

the oxygen atoms of the isocarbonyl ligands. In the case of $\mathbf{1}_{Dy}$ the Dy–C bond lengths lie in the range 2.618(13)–2.656(16) Å (average 2.631 Å) and the Dy–O bond lengths are 2.292(9) and 2.287(12) Å. The O-Dy-O angle is 87.5(5)°, the O-Dy-Cp_{cent} angles lie in the range 102.6(5)–104.2(5)° and the Cp_{cent}-Dy-Cp_{cent} angle is 141.5(3)° (Cp_{cent} = centroid of the Cp* ligand). The metallocene bending angle subtended at the dysprosium center in $\mathbf{1}_{Dy}$ is significant because it is approximately 11° greater than the analogous angles in other {Cp_2Dy}-based SMMs.[9–13] The coordination environment of the iron centers in $\mathbf{1}_{Dy}$ is essentially the same as those found in other Fp-containing complexes, with Fe-C(Cp) distances of 2.10(2)–2.12(2) Å (average 2.11 Å) and Fe-CO distances of 1.663(13) and 1.681(17) Å. The intramolecular Dy···Dy distance is 7.136(15) Å and the Fe···Fe distance is 7.232(15) Å. The geometric parameters of $\mathbf{1}_{Y}$ are very similar to those of $\mathbf{1}_{Dy}$ (Table S1). The IR spectra of $\mathbf{1}_{Y}$ and $\mathbf{1}_{Dy}$ (Figure S3) show two strong absorptions at 1721 and 1789 cm^{-1}, and at 1723 and 1793 cm^{-1}, respectively, as expected for two μ-isocarbonyl ligands in local C_{2v} symmetric environments.[15]

The magnetic properties of $\mathbf{1}_{Dy}$ were measured using a SQUID magnetometer. The plot of $\chi_M T(T)$ in an applied field of $H_{dc} = 10$ kOe (χ_M is the molar magnetic susceptibility) shows a monotonous decrease from 29.19 $cm^3 K mol^{-1}$ at 300 K down to approximately 25 K (Figure S5). At lower temperatures, a more rapid decrease in $\chi_M T$ occurs, with a value of 10.71 $cm^3 K mol^{-1}$ being reached at 2 K. The high temperature value of $\chi_M T$ is close to that of 28.34 $cm^3 K mol^{-1}$ predicted for two non-interacting Dy^{3+} ions with $^6H_{15/2}$ ground terms and $g_J = 4/3$, and the sharp drop at low temperatures is due to depopulation of the excited crystal field levels. The field dependence of the magnetization (Figure S5) at 1.8 K shows a rapid increase up to 10 kOe, before levelling off and reaching a saturation value of 10.78 $N_A\mu_B$ at 7 T.

The SMM properties of $\mathbf{1}_{Dy}$ were investigated using dynamic (a.c.) magnetic susceptibility measurements, with a small oscillating field of $H_{ac} = 1.55$ Oe and zero applied d.c. field. The in-phase (χ'; Figure S6) and out-of-phase (χ''; Figure 2) magnetic susceptibilities as a function of the a.c.

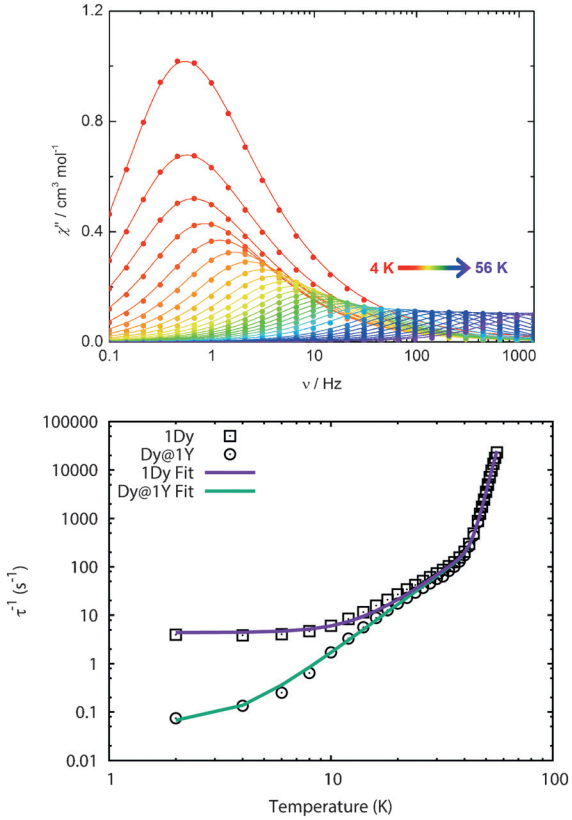

Figure 2. Top: $\chi''(\nu)$ at various temperatures in zero applied field for $\mathbf{1}_{Dy}$ (the solid lines are a guide for the eye). Bottom: temperature dependence of the relaxation time for $\mathbf{1}_{Dy}$ and **Dy@1**$_{Y}$ [the solid lines are fits of the data using Equation (1)].

frequency (ν) reveal prominent SMM behavior. Well-defined maxima were observed in the plot of $\chi''(\nu)$ at various temperatures in the range 4–56 K. Below 10 K, the peaks in $\chi''(\nu)$ occur at similar frequencies, but above 10 K the position of the maxima is strongly temperature dependent. The Argand plots of χ' versus χ'' (Figure S7) were fitted using a generalized Debye model in order to extract the magnetization relaxation times (τ). The α parameters are in the range 0.01–0.24, which indicates a narrow distribution of relaxation times. A magnetically diluted sample of 10% $\mathbf{1}_{Dy}$ doped into $\mathbf{1}_{Y}$ (**Dy@1**$_{Y}$) was also investigated, and it was found that the a.c. susceptibility data were virtually superimposable on those of $\mathbf{1}_{Dy}$ above 12 K (Figures S8, S9). At lower temperatures, the relaxation times for **Dy@1**$_{Y}$ are slower, due to suppression of QTM.

Insight into the dynamic magnetization of $\mathbf{1}_{Dy}$ was obtained through plots of τ^{-1} versus T (Figure 2; SI, Fig-

ure S10) and of ln τ versus T^{-1} (Figure S10). The temperature dependence of the relaxation time shows that the relaxation in $\mathbf{1_{Dy}}$ occurs over three distinct regimes. The high-temperature regime is dominated by an exponential process, that is, a multi-phonon Orbach process or thermally assisted quantum tunneling of the magnetization (TA-QTM); the low-temperature regime is dominated by QTM; and the intermediate regime is dominated by a Raman process.

We have fitted the data for both $\mathbf{1_{Dy}}$ and $\mathbf{Dy@1_Y}$ simultaneously using Equation (1), where τ_0^{-1} and U_{eff} are the Orbach parameters, C and n are the Raman parameters, and τ_{QTM}^{-1} is the QTM rate; the Orbach and Raman parameters were common to both data sets while the QTM parameters were different.

$$\tau^{-1} = \tau_0^{-1} e^{-U_{\text{eff}}/k_B T} + CT^n + \tau_{\text{QTM}}^{-1} \quad (1)$$

The best fit parameters were found to be $U_{\text{eff}} = 662(2)\ \text{cm}^{-1}$, $\tau_0 = 1.7(1) \times 10^{-12}$ s, $C = 7.7(3) \times 10^{-4}\ \text{s}^{-1}\text{K}^{-n}$, $n = 3.33(1)$, $\tau_{\text{QTM}}(\mathbf{1_{Dy}}) = 0.23(2)$ s and $\tau_{\text{QTM}}(\mathbf{Dy@1_Y}) = 17(3)$ s. The τ_0 parameter is in the expected range for Orbach relaxation over a large barrier, and despite the Raman exponent being low for a two-phonon process, such numbers have been observed recently for other dysprosium SMMs.[16] The U_{eff} value of 662(2) cm^{-1} (953 K) for $\mathbf{1_{Dy}}$ is the second largest for any type of SMM, being exceeded only by a recently reported pseudo-D_{5h}-symmetric Dy^{3+} complex.[16,17] For comparative purposes, the U_{eff} values extracted using only the high-temperature portion of relaxation data are 617 cm^{-1} and 583 cm^{-1} for $\mathbf{1_{Dy}}$ and $\mathbf{Dy@1_Y}$, respectively. The broader significance of $\mathbf{1_{Dy}}$ is that this SMM demonstrates that high-symmetry coordination environments are not an essential requirement for observing very large U_{eff} values.

The magnetic hysteresis properties of $\mathbf{1_{Dy}}$ were measured using a field sweep rate of 2.0 mT s^{-1}, which allowed S-shaped $M(H)$ hysteresis loops to be observed in the temperature range 1.8–6.2 K (Figure 3). At 1.8 K, the loops open at $|H| > 0$ and close at $H \approx \pm 10$ kOe. On approaching $H = 0$, the magnetization experiences a precipitous drop, in a manner that is characteristic of dysprosium SMMs and can be assigned to QTM. As the temperature of the measurement was increased in 0.8 K intervals to 6.2 K, the loops gradually closed. The hysteresis measurements on $\mathbf{Dy@1_Y}$ produced remarkably similar results to those recorded for $\mathbf{1_{Dy}}$, although the $M(H)$ loop around zero field is marginally wider in the dilute sample (Figure S11). Whereas the QTM rate of $\mathbf{Dy@1_Y}$ determined by a.c. susceptometry is almost two orders of magnitude slower than that of $\mathbf{1_{Dy}}$, there is essentially no discernible difference in their d.c. hysteresis profiles. This implies that the zero-field relaxation on the timescale of the hysteresis measurements is likely due to QTM arising from hyperfine interactions of the 4f electrons with spin-active dysprosium nuclei.[18]

To gain more insight into the magnetic properties of $\mathbf{1_{Dy}}$, we have performed complete active space self-consistent field (CASSCF) calculations on the experimentally determined geometry (see Supporting Information for details).[19] We observe that the four lowest energy KDs are highly anisotropic, displaying easy-axis anisotropy along a near co-linear direction. The main magnetic axis for the ground KD lies parallel with the $[Cp^*]_2$ coordination motif and at an angle of 80° with respect to the Dy_2Fe_2 mean plane, which is consistent with the model proposed in Scheme 1 (Figure S12). When the quantization axis for the crystal field decomposition is taken along this direction, it is clear that the ground KD is well described as the $m_J = \pm 15/2$ state of the $^6H_{15/2}$ multiplet (Table S3). Furthermore, the three subsequent excited states of the multiplet are also well described by the free-ion states $m_J = \pm 13/2$, $m_J = \pm 11/2$, and $m_J = \pm 9/2$, respectively. The four most energetic states of the multiplet are strong admixtures of the m_J functions, which results from the absence of a high-order symmetry axis.

By examining the average values of the matrix elements of magnetic moment connecting the electronic states (Figure 4), we deduce that the most probable thermally activated relaxation pathway involves spin-phonon excitation to the fourth-, fifth- or sixth excited doublets at 564, 580, and 639 cm^{-1}, respectively, followed by relaxation to the opposing ground state. Based on this data, it can be proposed that the extent to which the largest angular momentum states of Dy^{3+} in $\mathbf{1_{Dy}}$ are stabilized is a consequence of the magnetostructural correlation proposed in Scheme 1, that is, a combination of the Dy-Cp_{cent} distance, the Cp-Dy-Cp angles and the donor strength of the equatorial ligands.

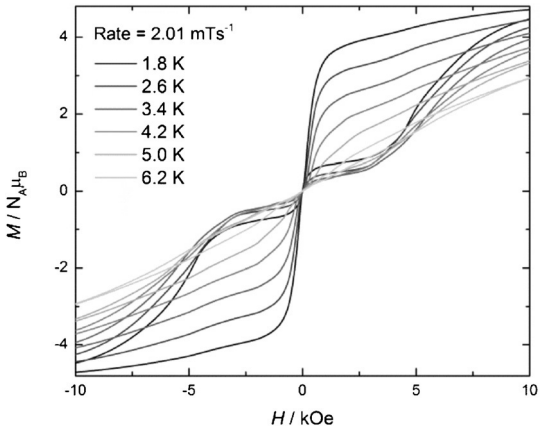

Figure 3. $M(H)$ hysteresis for $\mathbf{1_{Dy}}$ using a scan rate of 2.0 mT s^{-1}.

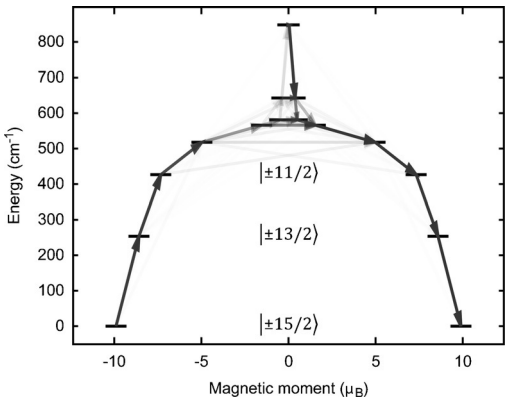

Figure 4. Calculated magnetic relaxation barrier for $\mathbf{1_{Dy}}$. Relaxation probabilities are calculated based on a magnetic perturbation and are normalized from each departing state.[7]

As the ground state of $\mathbf{1_{Dy}}$ can be defined by $m_J = \pm 15/2$, this SMM is amenable to electrostatic analysis with MAGELLAN.[20] In the electrostatic model, the orientation of the oblate electron density $\rho_{\pm 15/2}$, and thus the magnetic anisotropy axis, is determined by minimization of the electrostatic potential energy. Applying this to $\mathbf{1_{Dy}}$, each Cp* carbon donor atom is assigned a charge of −0.2, dysprosium is assigned a charge of +3, and the iscarbonyl ligands are neutral. The result is that the anisotropy axis predicted by the classical electrostatic model is essentially coincident with that calculated ab initio (deviation of 1.41°; Figures S12,13). The implication of this result is that the strong stabilization of the near-pure m_J states with the largest angular momenta in $\mathbf{1_{Dy}}$ is dominated by classical electrostatics, a feature that has also been observed in SMMs with highly symmetric dysprosium coordination environments.[21,22]

In conclusion, the SMM $[Cp^*_2Dy(\mu\text{-}Fp)]_2$ ($\mathbf{1_{Dy}}$) was targeted using a magnetostructural correlation in which the axial coordination sites are occupied by the strong-field $[Cp^*]^-$ ligands and the equatorial sites are occupied by weak-field, non-bulky isocarbonyl ligands. In zero field, maxima in $\chi''(\nu)$ were observed for $\mathbf{1_{Dy}}$ up to 56 K, and fitting the temperature dependence of the relaxation time allowed a very large U_{eff} value of 662 cm^{-1} to be extracted. Remarkably similar data were recorded for the magnetically dilute analogue $\mathbf{Dy@1_Y}$, although the dilution served to dramatically slow the QTM rate. Analysis of the magnetic properties of $\mathbf{1_{Dy}}$ using ab initio calculations revealed that the thermally activated relaxation processes occur via an unprecedented pathway via at least the fourth-excited Kramers doublet, and possibly also via the fifth- and sixth-excited states. In light of this result, efforts are now underway to develop SMMs that relax solely by going "over the top", that is, via the highest-lying Kramers doublet.[23]

Acknowledgements

R.A.L. thanks the European Research Council for the Consolidator Grant "RadMag" (646740), and the EPSRC for financial support.

Keywords: cyclopentadienyl ligands · dysprosium · molecular magnetism · organometallics · rare-earth elements

How to cite: *Angew. Chem. Int. Ed.* **2016**, *55*, 11082–11085
Angew. Chem. **2016**, *128*, 11248–11251

[1] a) J. M. Frost, K. L. M. Harriman, M. Murugesu, *Chem. Sci.* **2016**, *7*, 2470; b) P. Zhang, L. Zhang, J. Tang, *Dalton Trans.* **2015**, *44*, 3923; c) K. S. Pedersen, J. Bendix, R. Clérac, *Chem. Commun.* **2014**, *50*, 4396; d) D. N. Woodruff, R. E. P. Winpenny, R. A. Layfield, *Chem. Rev.* **2013**, *113*, 5110.

[2] J. D. Rinehart, M. Fang, W. J. Evans, J. R. Long, *J. Am. Chem. Soc.* **2011**, *133*, 14236.

[3] R. Vincent, S. Klyatskaya, M. Ruben, W. Wernsdorfer, F. Balestro, *Nature* **2012**, *488*, 357.

[4] C. Cervetti, A. Rettori, M. G. Pini, A. Cornia, A. Repollé, F. Luis, M. Dressel, S. Rauschenbach, K. Kern, M. Burghard, L. Bogani, *Nat. Mater.* **2016**, *15*, 164.

[5] a) E. Colacio, J. Ruiz, E. Ruiz, E. Cremades, J. Krzystek, S. Carretta, J. Cano, T. Guidi, W. Wernsdorfer, E. K. Brechin, *Angew. Chem. Int. Ed.* **2013**, *52*, 9130; *Angew. Chem.* **2013**, *125*, 9300; b) S. Gomez-Coca, E. Cremedes, N. Aliaga-Alcalde, E. Ruiz, *J. Am. Chem. Soc.* **2013**, *135*, 7010; c) Y. Rechkemmer, F. D. Breitgoff, M. van der Meer, M. Atanasov, M. Hakl, M, Orlita, P. Neugebauer, F. Neese, B. Sarkar, J. van Slageren, *Nat. Commun.* **2016**, *7*, 10467.

[6] a) Y.-C. Chen, J.-L. Liu, L. Ungur, J. Liu, Q.-W. Li, L.-F. Wang, Z.-P. Ni, L. F. Chibotaru, X.-M. Chen, M.-L. Tong, *J. Am. Chem. Soc.* **2016**, *138*, 2829; b) J. J. Le Roy, L. Ungur, I. Korobkov, L. F. Chibotaru, M. Murugesu, *J. Am. Chem. Soc.* **2014**, *136*, 8003; c) L. Ungur, J. J. Le Roy, I. Korobkov, M. Murugesu, L. F. Chibotaru, *Angew. Chem. Int. Ed.* **2014**, *53*, 4413; *Angew. Chem.* **2014**, *126*, 4502.

[7] a) N. F. Chilton, *Inorg. Chem.* **2015**, *54*, 2097; b) N. F. Chilton, C. A. P. Goodwin, D. P. Mills, R. E. P. Winpenny, *Chem. Commun.* **2015**, *51*, 101.

[8] a) R. A. Layfield, *Organometallics* **2014**, *33*, 1084; b) R. A. Layfield, J. J. W. McDouall, S. A. Sulway, D. Collison, F. Tuna, R. E. P. Winpenny, *Chem. Eur. J.* **2010**, *16*, 4442.

[9] T. Pugh, F. Tuna, L. Ungur, D. Collison, E. J. L. McInnes, L. F. Chibotaru, R. A. Layfield, *Nat. Commun.* **2015**, *6*, 7492.

[10] T. Pugh, V. Vieru, L. F. Chibotaru, R. A. Layfield, *Chem. Sci.* **2016**, *7*, 2128.

[11] T. Pugh, A. Kerridge, R. A. Layfield, *Angew. Chem. Int. Ed.* **2015**, *54*, 4255; *Angew. Chem.* **2015**, *127*, 4329.

[12] F. Tuna, C. A. Smith, M. Bodensteiner, L. Ungur, L. F. Chibotaru, E. J. L. McInnes, R. E. P. Winpenny, D. Collison, R. A. Layfield, *Angew. Chem. Int. Ed.* **2012**, *51*, 6976; *Angew. Chem.* **2012**, *124*, 7082.

[13] S. Demir, J. M. Zadrozny, J. R. Long, *Chem. Eur. J.* **2014**, *20*, 9524.

[14] CCDC 1473168 ($\mathbf{1_{Dy}}$) and 1473169 ($\mathbf{1_Y}$) contain the supplementary crystallographic data for this paper. These data can be obtained free of charge from The Cambridge Crystallographic Data Centre via www.ccdc.cam.ac.uk/data_request/cif.

[15] M. P. Blake, N. Kaltsoyannis, P. Mountford, *J. Am. Chem. Soc.* **2011**, *133*, 15358.

[16] J. Liu, Y.-C. Chen, J.-L. Liu, V. Vieru, L. Ungur, J.-H. Jia, L. F. Chibotaru, Y. Lan, W. Wernsdorfer, S. Gao, X.-M. Chen, M.-L. Tong, *J. Am. Chem. Soc.* **2016**, *138*, 5441.

[17] S. K. Gupta, T. Rajeshkumar, G. Rajaraman, R. Murugavel, *Chem. Sci.* **2016**, DOI: 10.1039/c6sc00279j.

[18] F. Pointillart, K. Bernot, S. Gohlen, B. Le Guennic, T. Guizouarn, L. Ouahab, O. Cador, *Angew. Chem. Int. Ed.* **2015**, *54*, 1504; *Angew. Chem.* **2015**, *127*, 1524.

[19] F. Aquilante, et al., *J. Comput. Chem.* **2016**, *37*, 506.

[20] N. F. Chilton, D. Collison, E. J. L. McInnes, R. E. P. Winpenny, A. Soncini, *Nat. Commun.* **2013**, *4*, 2551.

[21] a) I. Oyarzabal, J. Ruiz, J. M. Seco, M. Evangelisti, A. Camón, E. Ruiz, D. Aravena, E. Colacio, *Chem. Eur. J.* **2014**, *20*, 14262; b) I. Oyarzabal, J. Ruiz, E. Ruiz, D. Aravena, J. M. Seco, E. Colacio, *Chem. Commun.* **2015**, *51*, 12353.

[22] C. M. Dickie, M. Nippe, *Inorg. Chem. Front.* **2016**, *3*, 97.

[23] Note added in proof: A related study on metallocene SMMs was recently published: Y.-S. Meng, Y.-Q. Zhang, Z.-M. Wang, B.-W. Wang, S. Gao, *Chem. Eur. J.* **2016**, DOI: 10.1002/chem.201601934.

Received: May 4, 2016
Revised: June 7, 2016
Published online: July 27, 2016

